X-ray radiography based on the phase-contrast imaging with using LiF detector

S S Makarov, T A Pikuz, A V Buzmakov, A P Chernyaev, P Mabey, T Vinci, G Rigon, B Albertazzi, A Casner, V Bouffetier, et al.

X-ray radiography based on the phase-contrast imaging with using LiF detector

X-ray radiography based on the phase-contrast imaging with using LiF detector

S S Makarov[1,2], T A Pikuz[1,3], A V Buzmakov[4], A P Chernyaev[2], P Mabey[5], T Vinci[5], G Rigon[5], B Albertazzi[5], A Casner[6], V Bouffetier[6], R Kodama[7], K Katagiri[7], N Kamimura[7], Y Umeda[7], N Ozaki[7,8], E Falize[9], O Poujade[9], T Togashi[10,11], M Yabashi[10,11], T Yabuuchi[10,11], Y Inubushi[10,11], K Miyanishi[11], K Sueda[11], M Manuel[12], G Gregori[13], M Koenig[5] and S A Pikuz[1,14]

[1] Joint Institute for High Temperatures of the Russian Academy of Sciences, Izhorskaya 13 Bldg 2, Moscow 125412, Russia
[2] Department of Physics, Lomonosov Moscow State University, Leninskiye Gory 1 Bldg 2, Moscow 119991, Russia
[3] Open and Transdisciplinary Research Initiative, Osaka University, 2-1 Yamadaoka, Suita, Osaka 565-0871, Japan
[4] Federal Scientific Research Centre "Crystallography and Photonics" of the Russian Academy of Sciences, Leninsky Avenue 59, Moscow 119333, Russia
[5] Laboratoire pour l'Utilisation des Lasers Intenses, CNRS-CEA, École Polytechnique, Physique Atomique dans les Plasmas Denses, Route de Saclay, Palaiseau F-91128, France
[6] Centre National de la Recherche Scientifique, Rue Michel Ange 3, Paris 75016, France
[7] Graduate School of Engineering, Osaka University, 2-1 Yamadaoka, Suita, Osaka 565-0871, Japan
[8] Institute of Laser Engineering, Osaka University, 2-6 Yamadaoka, Suita, Osaka 565-0871, Japan
[9] Commissariat à l'Energie Atomique, Centre DAM Ile de France, Bruyères le Châtel, France
[10] Japan Synchrotron Radiation Research Institute, 1-1-1, Kouto, Sayo-cho, Sayo-gun, Hyogo 679-5198, Japan
[11] RIKEN SPring-8 Center, 1-1-1, Kouto, Sayo-cho, Sayo-gun, Hyogo 679-5148, Japan
[12] Inertial Fusion Technologies, General Atomics, P.O. Box 85608, San Diego, CA 92186, United States
[13] Department of Physics, University of Oxford, Parks Road, Oxford OX1 3PU, United Kingdom (Great Britain)
[14] National Research Nuclear University MEPhI (Moscow Engineering Physics Institute), Kashirskoe Shosse 31, Moscow 115409, Russia

E-mail: seomakarov28@gmail.com

Abstract. An x-ray radiography technique based upon phase contrast imaging using a lithium fluoride detector has been demonstrated for goals of high energy density physics experiments. Based on the simulation of propagation an x-ray free-electron laser beam through a test-object, the visibility of phase-contrast image depending on an object-detector distance was investigated. Additionally, the metrological capabilities of a lithium fluoride crystal as a detector were demonstrated.

1. Introduction

Today, a field of high energy density physics (HEDP) is actively developing and exploring tasks including laboratory astrophysics [1, 2], materials science [3] and inertial confinement fusion research [4, 5]. This is facilitated by the appearance of high-intensity optical lasers and fast Z-pinch sources capable of heating matter to extreme conditions (density, temperature, velocity).

X-ray radiography is widely used to visualize the processes that are studied in experiments in high energy density physics. A technique of absorption contrast is used for conventional x-ray radiography of objects. However, the absorption on the hard x-ray photons, which used in HEDP experiments, is very weak to see distinct images. An alternative approach to investigate low absorbing objects is phase-contrast imaging (PCI) radiography [6].

Variations in the thickness and refractive index of the test object lead to a change in the intensity and phase shift of the x-ray wavefront passing through the object. A phase-contrast enhancement occurs at the object boundary, depending on the phase shift of the field associated with the thickness of the object, and an object-to-detector distance. Despite the fairly low absorption for the hard x-ray, contrast can be improved by moving a detector at some distance from the investigated object, resulting in an intensity jump appears at the areas with a density gradient, indicating an increased contrast.

The high spatial coherence of the x-ray source is a key requirement for the PCI technique. The brightest examples of capabilities this approach were demonstrated in [7–10]. The Talbot–Lau x-ray deflectometry (TXD) phase retrieval methods (phase stepping and single-shot Moire deflectometry) were successfully used in the context of HED plasma characterization for an electron density retrieval [7, 8]. The phase-contrast imaging of shock waves and wire explosion dynamics in HEDP experiments with a spatial resolution of 8 μm was shown in work [9] by using of synchrotron radiation (European Synchrotron Radiation Facility, France) as a probe beam.

In many cases, the selection of the correct detector is critical in ensuring high image quality. One of the most important requirements for a detector in HEDP experiments is the simultaneous provision of micron (submicron) spatial resolution, a wide dynamic range, and a large field of view. A charge-coupled device (CCD) as conventionally used detector often cannot satisfy this requirement when recording images in super-intense x-ray fields. The photoluminescent detectors are considered extremely promising for the registration of super-intensive x-ray beams. In recent work [11] the capabilities of novel x-ray imaging detectors utilizing an Ag-doped phosphate glass and lithium fluoride (LiF) films were demonstrated for their applications in the two-dimensional (2D) dose imaging. The advantages of such detectors compared to image plates (IP) are a high spatial resolution on the order of microns, a wide dynamic range and a non-destructive signal readout operation. Using the combination of laser-plasma x-ray sources as backlighter with a LiF detector for the tasks of x-ray radiography of nanothickness foils and biological objects were performed in works [10, 12–15].

The purpose of this paper is to demonstrate the capabilities of x-ray radiography based on the phase-contrast imaging in HEDP experiments with using LiF detector.

2. Phase-contrast imaging scheme

The phase-contrast imaging greatly increases the information content of the images. It enables observation of weakly or non-absorbing objects and the high-spatial frequency feature, such as edges and sharp density gradients. The phase-contrast enhancement in the image is defined by the phase shift of x-ray photons deflected from higher density region to lower density region. At the optimal conditions, it appears in the image as a characteristic black-white diffraction fringe. For the given photon energy the achievable contrast strongly depends on an object-to-detector distance.

Modulated targets are widely used in experiments to study the Rayleigh–Taylor instability (RTI) observed in laboratory astrophysics [16–18]. To get close to the best observation of the

phase-contrast imaging regime under our experimental conditions we have modeled an x-ray free-electron laser (XFEL) beam propagation through the real RTI target. The simulations have been done using the method developed in [16] applying open-access code WavePropaGator (WPG) [19, 20].

In our modeling, the XFEL beam with a photon energy of 7 keV irradiates the object directly without focusing (SPring-8 Angstrom Compact free electron laser—SACLA, Japan). Divergence of the beam is taken of 2.4 μrad, the size of the beam in the plane of an object is 1 mm (in full width at half maximum) and intensity profile is Gaussian. The object is a complex three-dimensional (3D) RTI target consists of a layer of brominated plastic (C_8H_7Br, density 1.54 g/cm^3), polyamide cylinder with a diameter of 1 mm (the wall thickness of 40 μm), which enfolds the brominated layer, and a low-density foam (a resorcinol formaldehyde ($C_{15}H_{12}O_4$), density 100 mg/cm^3) which fills the cylinder and attaches the brominated layer. A brominated layer has an initial profile of the ripples with a period of 120 μm and top-value amplitude of 40 μm.

To construct the transmission function of this composite object, we first split the object into two parts: cylinder from polyamide and cylinder from materials created interface. Then for each part of the target, we built a 3D numerical model and integrated it to obtain the 2D transmission functions, including absorption and wavefront phase shift. The resulting transmission function of the whole object was taken into account as

$$T(x, y, \omega) = \int T_{\text{cyl}}(x, y, z, \omega)\mathrm{d}z \int T_{\text{int}}(x, y, z, \omega)\mathrm{d}z, \tag{1}$$

where $T_{\text{cyl}}(x, y, z, \omega)$ and $T_{\text{int}}(x, y, z, \omega)$ are the complex transmission functions of cylinder and interface, respectively; z is the axis of XFEL beam propagation, which is perpendicular to the observation plane; is the angular frequency.

After setting the incident beam and the object transmission function, we used WPG code to simulate the propagation of the XFEL beam over the different distances R behind the object in the range of 10–200 mm. The results of the simulation are shown in figure 1. As one can see, the phase-contrast enhancement in the image of the interface becomes visible at the distances R more 40 mm. With the increase of distance R the intensity of the phase-contrast peak gradually increases. At the distances R = 80–120 mm, a single narrow fringe is well pronounced, while the width of the fringe is in order of 1 μm. At the larger distances, the width of the main peak increases and the intensity of high-frequency fringes growing. The large width of the first phase-contrast peak and presents of high order modulations may reduce the spatial resolution of the imaging scheme. Indeed to resolve the two density steps at the distance a, the full width at half maximum (FWHM) of the edge intensity envelope needed to be equal or smaller than a. Thus, we conclude that at the distances R = 100–120 mm the imaging scheme will satisfy both requirements: providing conditions for observing phase-contrast and achieving the spatial resolution of 1 μm.

3. LiF crystal as x-ray imaging detector

LiF is a photoluminescence detector. In the volume of LiF crystalline structure, the ionization radiation generates F-type color centers (CCs), in particular, F_3 and F_2 color centers, figure 2(a), which are quite uniquely stable at the room temperature and may survive for many years with a very low rate of decay [21, 22]. The bandgap of LiF is 14 eV, while it is sensitive to the wide range of photon energy from extreme ultraviolet range (EUV) to hard x-ray. After the exposure, the hidden images formed by CCs are stored in the crystal. The excitation bands for both types of color centers is almost fully overlapped in the spectral range 400–500 nm, figure 2(b). The emission band starts from a wavelength of 510 nm and has the central wavelength 540 nm and 670 nm for F_3 and F_2 CCs, correspondently, see figure 2(b). So to observe the recorded image

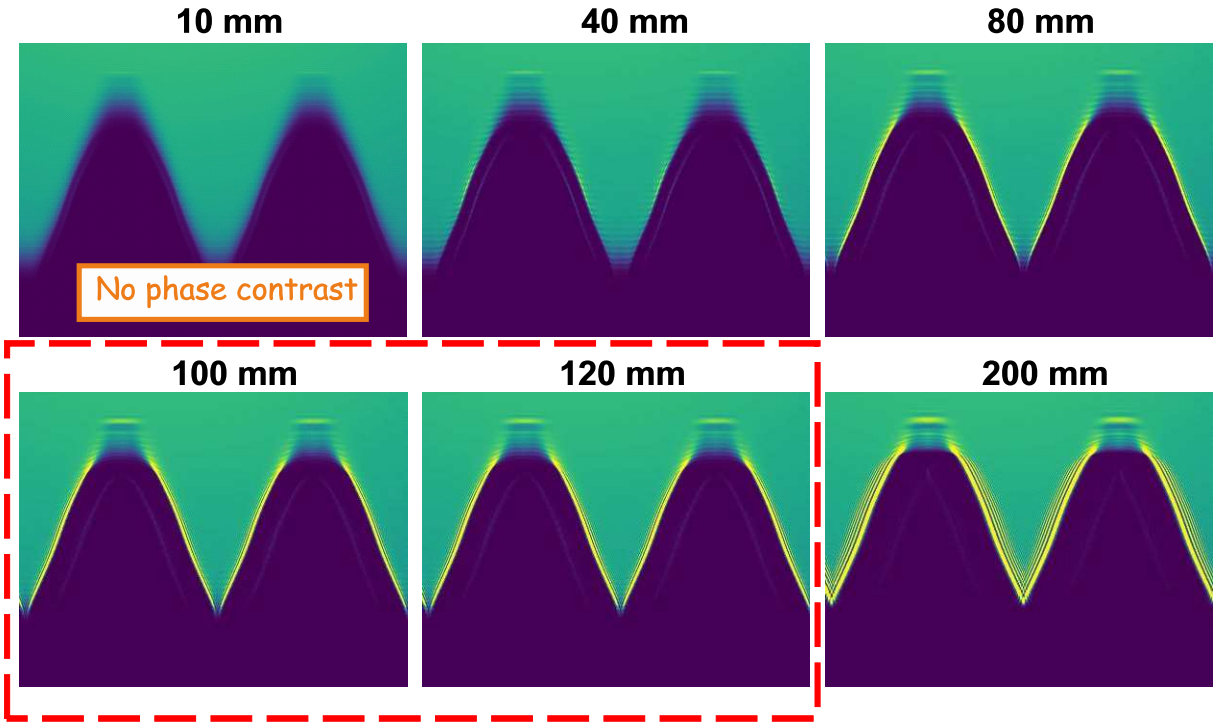

Figure 1. Simulation of the enhancement of the phase contrast image for a RTI static target at different distances "target-to-detector" $R = 10$–200 mm.

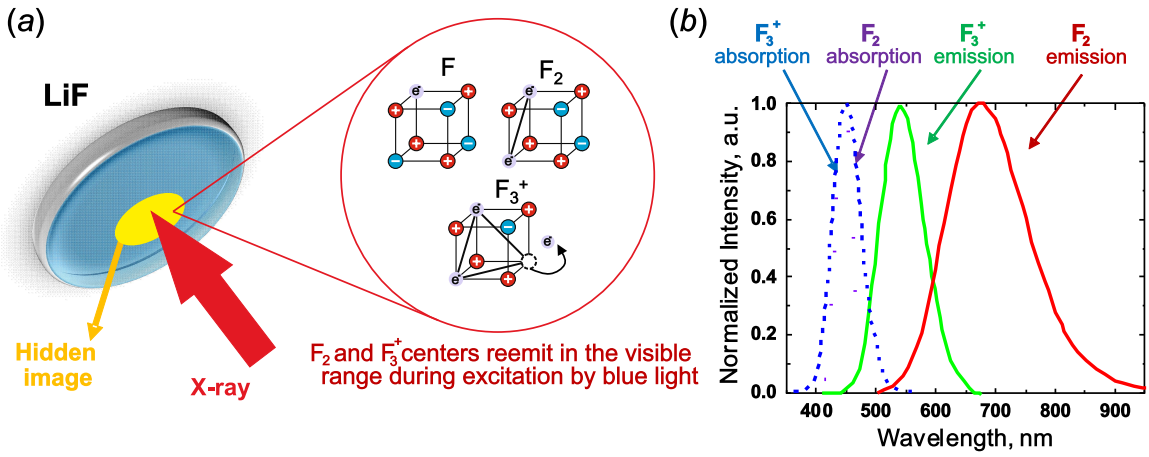

Figure 2. Formation of image in the LiF detector: (a) generation of color centers in LiF crystal; (b) absorption and emission bands of F_2 and F_3 color centers in LiF.

in the photoluminescence (PL) emission of CCs conventional readout systems like fluorescent microscope can be applied. The density of CCs is proportional to the x-ray absorbed dose. Larger the dose rate is deposited, higher is the coloration efficiency achieved. The x-ray radiation, attenuated by the object, produces CCs, whose density is proportional to the intensity of the radiation transmitted through the same object.

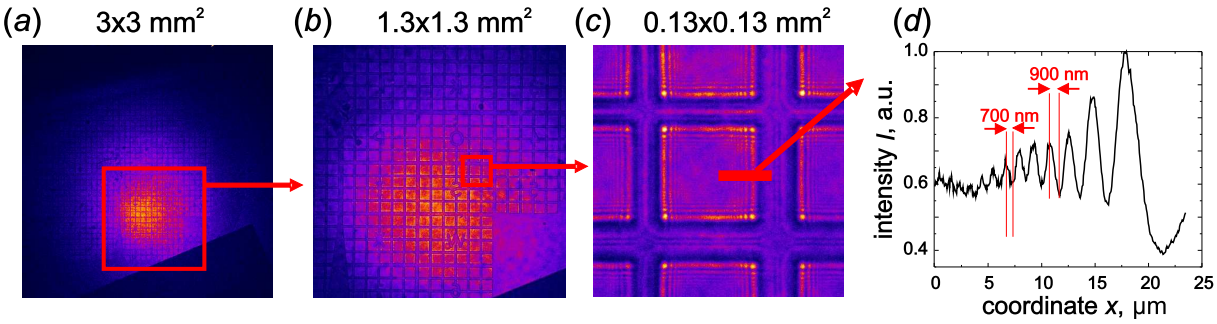

Figure 3. X-ray radiography image of the test mesh obtained on the LiF detector with different magnification: (*a*) 4×, (*b*) 10× and (*c*) 100×; (*d*) profile of experimental diffraction pattern taken along red line in (*c*).

3.1. Spatial resolution

Potentially, the spatial resolution of the LiF crystal is of the order of CCs size scale (atom scale). However, in practice, it is limited by two factors. First is the resolution of the readout system. With the use of a confocal fluorescent microscope with dry objective (without emersion) the optical resolution can be close to 200 nm. Second is the size of electron cloud generated by hard x-ray radiation. The physics of this process depending on x-ray energy is described in details in [23]. For our case of the photon energy of 7 keV the estimations are given in [24] suggested the value of 600 nm. Experimentally achieved spatial resolution is close to that value. Radiography image of Ni mesh with a period of 63 μm irradiated by direct SACLA beam with a photon energy of 7 kev is shown, in figure 3. The observed LiF image was read-out at various magnifications of a microscope. It is seen that the diffraction pattern high order diffraction fringes with the width down to 700 nm have been resolved, see figure 3(*c, d*).

3.2. Field of view

The field of view of LiF detector alternatively defined by two factors: the size of LiF plate and the size of the beam that irradiates the object and imaged the object on the detector. A LiF is a convenient optical material. The plates of the LiF may have sizes of tens cm^2. In our experiment, the field of view corresponded to the size of the XFEL beam. In the experimental hutch EH5 (SACLA facility), the beam delivered from the frontend to the target plane has the size of 700 μm (FWHM), while the number of the photons within the radius of 1.5 mm is enough to measure the signal with the spatial resolution of 700 nm on the LiF in one shot, see figure 3(*a*). Thus, in our experimental conditions, the LiF detector allows obtaining extremely large image-size-to-resolution ratio 4000.

3.3. Dynamic range

The dynamic range of LiF crystal exceeds the value of 16-bit, which is typical for conventional detectors. The bright example demonstrates it in [25] from the experiment at the synchrotron source PETRA III (Deutsches Elektronen-Synchrotron, Germany).

Top part of figure 4 shows the image of a pinhole diffraction pattern obtained on the LiF with a different gain of microscope photomultiplier in the mentioned work. The difference between photoluminescence (PL) intensity in the central maximum and the periphery much exceeded the dynamic range of microscope detector (16-bit). As seen, the PL intensity in the central maximum measured by microscope without saturation (gain 360) the high order maximum of diffraction pattern cannot be recognized (left panel image). Strong saturation of the central

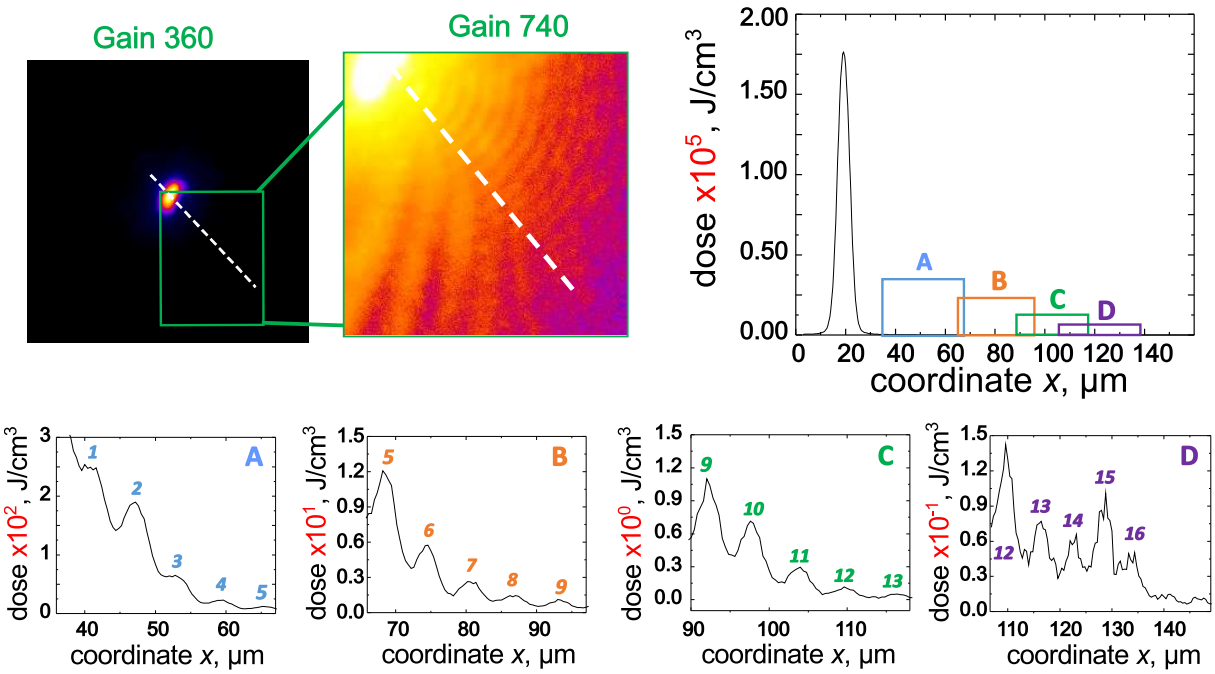

Figure 4. The result of an experiment to reveal the LiF dynamic range in the field of synchrotron radiation [25]: (left upper panel image)—Image of pinhole diffraction pattern obtained on the LiF with different gain of photomultiplier and (right and down panel)—dose distribution profile in LiF detector profile taken along white dash-line (the numbers 1–16 on the A–D panels indicate the observed diffraction maxima).

peak by an increase of the gain up to 740 allowed visualizing the diffraction rings up to 16th diffraction order (right panel image). The dynamic range of LiF detector was considered as the ratio $D_{\max}$ to $D_{\min}$, where $D_{\max}$ and $D_{\min}$ are the accumulated doses correspondent to maximal and minimal observed PL signal in the diffraction pattern. Correspondent to the PL intensity doses are shown in the plots A–D. The ration between the doses accumulated in the central peak of 1.7×10^5 J/cm^3 and in the last observed ring (16th) of 3×10^{-2} J/cm^3 is about 10^6. This value is at least two orders larger compare to the dynamic range of image plates, scintillator based detectors and charge-coupled devices.

3.4. Property of self-filtering

One of the problems arising in the pump-probe experiments is the background x-ray radiation from plasma generated when the pumping laser interacts with the target. It can significantly worsen the signal-to-noise ratio in the radiography image. Various filters are used to minimize this effect, which can further distort the incident wavefront of a probe laser. The LiF detector allows mitigating this problem without the use of any filters. The CCs are generated in the whole depth along with the beam propagation until the incident radiation will be absorbed. In the spectral range of LiF sensitivity, the attenuation length is changing from tens of nanometers in EUV spectral range to millimeters for a hard x-ray. This means that background soft x-ray radiation is absorbed in the top layer of the detector, and the hard radiation penetrates in deeper layers. Thus, it is possible to reduce the negative effect of background soft x-ray radiation in the observed image, if reading a signal from the depth of the LiF crystal by using a confocal microscope.

4. Conclusions

X-ray radiography based on the phase-contrast imaging is a perspective method for the goals of HEDP experiments. The using of lithium fluoride crystal as a detector in such method can significantly improve the image quality of the investigated object or process. This detector allows to register the image with submicron spatial resolution, the field of view up to tens cm^2 and high dynamic range (not less 10^6).

Acknowledgments

The reported study was funded by the Russian Foundation for Basic Research, project No. 19-32-90142. Also, the work was done in the frame of the state assignment of the Ministry of Science and Higher Education to the Joint Institute for High Temperatures of the Russian Academy of Sciences.

References

[1] Suttle L G *et al* 2018 *Phys. Plasmas* **25** 042108
[2] Remington B A, Drake R P and Ryutov D D 2006 *Rev. Mod. Phys.* **78** 755–807
[3] Maire E, Buffire J Y, Salvo L, Blandin J J, Ludwig W and Letang J M 2001 *Adv. Eng. Mater.* **3** 539–46
[4] Zhang X, Wang G, Zhaoa J, Tan F, Luo B and Sun C 2014 *Rev. Sci. Instrum.* **85** 055110
[5] Lindl J D *et al* 2004 *Phys. Plasmas* **11** 339–491
[6] Wilkins S W, Gureyev T E, Gao D, Pogany A and Stevenson A W 1996 *Nature* **384** 335–8
[7] Valdivia M P, Stutman D, Stoeckl C, Mileham C, Begishev I A, Bromage J and Regan S P 2018 *Appl. Opt.* **57** 138–45
[8] Valdivia M P *et al* 2020 *Rev. Sci. Instrum.* **91** 023511
[9] Theocharous S P, Bland S N, Yanuka D, Rososhek A, Olbinado M P, Rack A and Krasik Ya E 2019 *Rev. Sci. Instrum.* **90** 013504
[10] Gasilov S *et al* 2009 *Contrib. Plasma Phys.* **49** 488–95
[11] Kurobori T, Miyamoto Y, Maruyama Y, Yamamoto T and Sasaki T 2014 *Nucl. Instrum. Methods Phys. Res., Sect. B* **326** 76–80
[12] Hampai D, Dabagov S B, Ventura G D, Bellatreccia F, Magi M, Bonfigli F and Montereali R M 2011 *EPL* **96** 60010
[13] Baldacchini G *et al* 2003 *J. Nanosci. Nanotechnol.* **3** 483–6
[14] Reale L *et al* 2015 *J. Microsc.* **258** 127–39
[15] Fukuda Y *et al* 2008 *Appl. Phys. Lett.* **92** 121110
[16] Faenov A Ya *et al* 2018 *Sci. Rep.* **8** 16407
[17] Rigon G *et al* 2019 *Phys. Rev.* E **100** 021201
[18] Casner A *et al* 2019 *Nucl. Fusion* **59** 032002
[19] Samoylova L, Buzmakov A, Chubar O and Harald S 2016 *J. Appl. Crystallogr.* **49** 1347–55
[20] Chubar O, Couprie M, Labat M, Lambert G, Polack F and Tcherbakoff O 2008 *Nucl. Instrum. Methods Phys. Res., Sect. A* **593** 30–4
[21] Baldacchini G *et al* 2005 *Rev. Sci. Instrum.* **76** 113104
[22] Voitovich A P *et al* 2011 *J. Appl. Spectrosc.* **77** 857–68
[23] Grum-Grzhimailo A N *et al* 2017 *Eur. Phys. J. D* **71** 69
[24] Pikuz T A *et al* 2015 *Sci. Rep.* **5** 17713
[25] Makarov S S *et al* 2020 *J. Synchrotron Radiat.* **27** 625–32